# Network Experimental Workflow Leveraging MDE and LLM: Case Study of Wireless System Performance in an α-μ Fading Environment with Selection Diversity Receiver

Dragana Krstic
University of Nis, Faculty of Electronic Engineering
Nis, Serbia
Email: dragana.krstic@elfak.ni.ac.rs

Suad Suljovic
Academy of Applied Technical Studies Belgrade
Belgrade, Serbia
Email: ssuljovic@atssb.edu.rs

Nenad Petrovic
University of Nis, Faculty of Electronic Engineering
Nis, Serbia
Email: nenad.petrovic@elfak.ni.ac.rs

Goran Djordjevic
Academy of Applied Technical Studies Belgrade
Belgrade, Serbia
Email: gdjordjevic@atssb.edu.rs

Devendra S. Gurjar
Department of Electronics and Communications Engineering, National Institute of Technology Silchar
Assam, India
Email: dsgurjar@ece.nits.ac.in

Suneel Yadav
Department of Electronics and Communication Engineering, Indian Institute of Information Technology Allahabad
Email: suneel@iiita.ac.in

***Abstract*—In this paper, a wireless system in the presence of α-μ fading and Co-Channel Interference (CCI) is observed. CCI, a sort of congestion in wireless systems, often has the same distribution as the fading in the observed environment. The α−μ distribution used here is a common model for small-scale fading of THz links. We used diversity receiver with Selection Combining (SC) to mitigate these adverse effects of fading and CCI. For wireless system configured with SC receiver, we derived the Average Bit Error Probability (ABEP) based on the Moment Generating Function (MGF), the level crossing rate (LCR), the average fade duration (AFD), and the channel capacity (CC). The analytical results are presented in a greater number of graphics to highlight the parameters' influence of fading and CCI. Additionally, we propose a workflow for convenient network planning leveraging the synergy of Large Language Models (LLMs) and model-driven engineering (MDE) approach, making use of the previously derived expressions within the evaluation scenario.**

***Keywords- α-μ fading; Co-Channel Interference (CCI); Large Language Model (LLM); Model-driven engineering (MDE); Selection Combining (SC).***

## I. INTRODUCTION

Among the most critical disturbances of signal propagation in wireless channels is fading. Describing and modeling of wireless channels in the presence of fading is of particular importance as for designing the transmission system itself, as well as for the performance analysis. During the development of wireless communications, a large number of different channel fading distribution models have been defined to describe correctly the statistical characteristics of the amplitude and phase of the propagated signal. In the last few years, a general fading distributions are the most popular because other known distributions can be obtained from them. Between them are: α-μ, κ-μ, η-μ, α-κ-μ, α-η-μ, λ-μ, etc. [1]-[7].

In this work, the α-μ distribution is introduced to model a small-scale fading. Usage of α−μ distribution is a common model for small-scale fading of THz links. With this distribution, the nonlinearity of the propagation medium is included since the premise of homogeneity is unrealistic and only approximates the actual transmission medium [2]. As said, α-μ distribution is general distribution. This is generalized Gamma distribution that includes other distributions as are: Gamma (with Erlang as its discrete versions, and also central Chi-squared), Nakagami-*m* (with its discrete version- Chi distribution), Rayleigh, exponential, Weibull, and One-sided Gaussian [3]. That is why it is suitable for an analysis of the performance of wireless systems in the presence of the listed types of fading. The performance obtained for α-μ fading can be reduced to special cases of those fading's distributions obtained for specified values of parameters α and μ.

There are still not many works in the literature that consider this fading distribution, although it is very suitable. Some of them are [8] - [13].

In [8], the Moment Generating Function (MGF) for the Probability Density Function (PDF) of an α-μ wireless fading channel is evaluated for non-integer values of α. By dint of the MGF, the Bit Error Rate (BER) for different modulation techniques is derived. Also, formula for the outage probability (Pout) in the closed form is obtained. All obtained expressions can be reduced to the special cases of Nakagami-*m*, Rayleigh, and Weibull fading channels. The same authors in [9] derived expressions for the amount of

fading and the average channel capacity (CC) for α-μ wireless fading channel.

In [10], the authors proposed a novel MGF for α-μ fading distribution valid for all values of parameter α, as an improvement of [8]. Then, the BER expressions in closed-form are derived for different modulation techniques such as Binary Phase-Shift Keying (BPSK), Binary Frequency Shift Keying (BFSK), Differential Quadrature PSK (DQPSK), Binary Differential PSK (BDPSK), and *M*-ary PSK (MPSK) over α-μ fading channels.

An enriched $\alpha-\mu$ distribution is observed in [11] because it also can be convenient for fading model. Further, in [12], the authors analyzed the complex α-μ fading channel with an application in Orthogonal Frequency-Division Multiplexing (OFDM) systems.

The expressions for the PDF and Cumulative Distribution Function (CDF) of the square ratio of two multivariate exponentially correlated variables with α-μ distribution are determined in [13]. These formulas provide the basis for analyzing system performance in the presence of interference, based on the Signal-to-Interference Ratio (SIR), when using a Selection Combining (SC) receiver to reduce the effects of fading and interference.

The Co-Channel Interference (CCI) also occurs in wireless systems beside fading when more than one device is operating on the same frequency channel. Its influence has to be studied along with the influence of fading [14].

Our group of authors introduce CCI into analysis and made a few papers with this topic. So, in [15], an analysis of outage probability for selection combining (SC) receiver under the influence of α−μ fading and α−μ CCI is presented. The derived PDF and Pout are shown graphically. The fading and CCI parameters impact is highlighted. After, the simulation software environment for modelling and planning of wireless MIMO systems with *L*-branch SC receiver under the influence of α−μ fading and CCI is given in order to minimize the transmission costs and have the best possible Quality of Service (QoS) for defined data transfer scenario.

We performed in [16] the channel capacity of such *L*-branch SC receiver under the α−μ small-scale fading and CCI with the same distribution. The analytical results for the CC was derived in the closed form. Then, some graphs are plotted to highlight the magnitude of the disturbance. In addition, quantum computing-based machine learning approach to service consumer number prediction and Quality of Service (QoS) level estimation leveraging the previously calculated channel capacity value using Qiskit library in Python is introduced. In [17], the Level Crossing Rate (LCR) of MIMO systems with *L*-branch selection combining (SC) receiver in the presence of α-μ fading and α-μ CCI effects during transmission, is derived. After, an accelerated graphics processing unit (GPU) simulation is applied to plan a QoS-efficient 5G mobile network in a smart city. The goal is to optimize the LCR calculation speed for the observed communication system type, by providing efficient planning (reducing costs and maximizing performance) with combined approach of linear optimization and deep learning.

In this paper, we perform different performance of an α-μ fading and CCI environment when SC diversity receiver was used to mitigate the influences of these disturbances. Among them are: a MGF-based calculation of the Average Bit Error Probability (ABEP), the level crossing rate (LCR), the average fade duration (AFD), and the channel capacity. According to our knowledge, the derivation of these performance for the scenario defined here has not been reported in available literature.

Afterwards, an experimental workflow aiming to make network planning faster, relying on model-driven engineering (MDE) – for network model representation and Large Language Models (LLM) – for generating experiment code based on textual description. In this context, the expression derived in the first part of the paper is used for approach evaluation.

This work consists of six sections. After the introduction, in Section II, the SIR-based analysis of the performance of SC receiver in the presence of α-μ fading and CCI is presented, and that: PDF of the output SIR, moment generating function, ABEP for BFSK modulation and BDPSK modulation. In Section III, the second order system performance (LCR and AFD) are obtained, and channel capacity is presented in Section IV. In Section V, LLM-enabled wireless network planning workflow is done, and Section VI concludes the paper.

## II. SIR- BASED PERFORMANCE ANALYSIS

We derive in the next parts of the paper the performance of a wireless system in the presence of α-μ fading and CCI. To mitigate the effects of fading and CCI, a SC diversity receiver with *L* branches is utilized. This receiver is shown in Figure 1. The SC receiver works so that transmits to the user the signal from the input with the highest value.

We have labeled the inputs with: $x_i$, $i$=1, 2, …, $L$; $L \geq 2$, and the output signal with $x$. The CCI input envelopes are $y_i$, $i$=1, 2, …, $L$ with output value $y$. Considering the presence of CCI, performance will be determined on the basis of output SIR, denoted by $z$. Input SIRs are equal to the ratios of the useful signals and the CCIs at the input antennas ($z_i = x_i / y_i$).

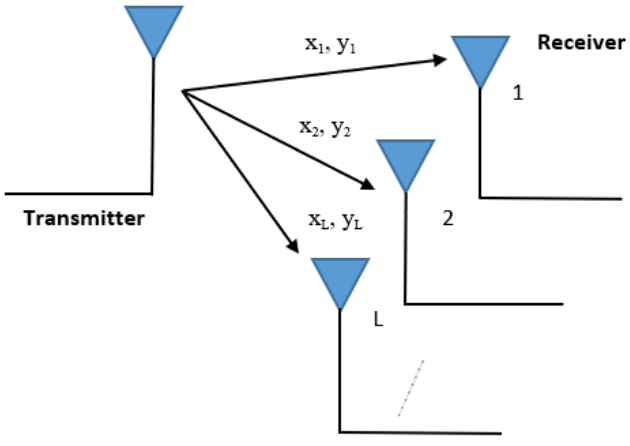


Figure 1. Model of a selection combining diversity receiver.

### A. The PDF of the Output SIR

The useful signal has the α-μ distribution [3]:

$$p_{x_i}(x_i) = \frac{\alpha \mu_1^{\mu_1} x_i^{\alpha\mu_1 - 1}}{\Omega_i^{\mu_1}\Gamma(\mu_1)} \mathrm{e}^{-\mu_1 \frac{x_i^{\alpha}}{\Omega_i}} . \quad (1)$$

The parameters are: $\alpha$ (describes the nonlinearity of the propagation environment), $\mu_j$ (shows the number of clusters in that environment and the indices are: $j$=1 for the signal, and $j$=2 for the CCI), and $\Omega_i$, $i$=1, 2, …, $L$, (the mean values of the input signals powers). $\Gamma(\cdot)$ denotes the Gamma function.

The CCI also follows α-μ distribution:

$$p_{y_i}(y_i) = \frac{\alpha \mu_2^{\mu_2} y_i^{\alpha\mu_2 - 1}}{s_i^{\mu_2}\Gamma(\mu_2)} \mathrm{e}^{-\mu_2 \frac{y_i^{\alpha}}{s_i}} , \quad (2)$$

where $s_i$ marks the average powers of the CCI.

The PDFs of the SIRs $z_i$ are given as [18]:

$$p_{z_i}(z_i) = \int_0^{\infty} y_i \, p_{x_i}(z_i y_i) \, p_{y_i}(y_i) \, dy_i . \quad (3)$$

If we substitute (1) and (2) into (3), the PDFs for SIRs are obtained as:

$$p_{z_i}(z_i) = \frac{\alpha \mu_1^{\mu_1} \mu_2^{\mu_2} z_i^{\alpha\mu_1 - 1} \Omega_i^{\mu_2} s_i^{\mu_1} \Gamma(\mu_1 + \mu_2)}{\Gamma(\mu_2)\Gamma(\mu_1)\left(\Omega_i \mu_2 + \mu_1 s_i z_i^{\alpha}\right)^{\mu_1 + \mu_2}} . \quad (4)$$

From the next formula [18], it is possible to derive the expression for CDF of $z_i$:

$$F_{z_i}(z_i) = \int_0^{z_i} p_{z_i}(t) \, dt . \quad (5)$$

After substitution (4) into (5), the CDF of the SIR $z_i$ is:

$$F_{z_i}(z_i) = \frac{\alpha (\mu_1 s_i)^{\mu_1} (\mu_2 \Omega_i)^{\mu_2}}{\Gamma(\mu_2)} \cdot \frac{\Gamma(\mu_1 + \mu_2)}{\Gamma(\mu_1)} \times$$

$$\times \int_0^{z_i} \frac{z_i^{\alpha\mu_1 - 1}}{\left(\Omega_i \mu_2 + \mu_1 s_i z_i^{\alpha}\right)^{\mu_1 + \mu_2}} dt . \quad (6)$$

The integral from (6) is solved by using Beta function [19]:

$$\int_0^{\lambda} \frac{x^m}{\left(a + b x^n\right)^p} dx = \frac{a^{-p}}{n} \left(\frac{a}{b}\right)^{\frac{m+1}{n}} B_z\left(\frac{m+1}{n}, p - \frac{m+1}{n}\right)$$

$$z = \frac{b\lambda^n}{a + b\lambda^n}, a > 0, b > 0, n > 0, 0 < \frac{m+1}{n} < p . \quad (7)$$

Finally, the CDF of $z_i$ is in the form:

$$F_{z_i}(z_i) = \frac{\Gamma(\mu_1 + \mu_2)}{\Gamma(\mu_2)\Gamma(\mu_1)} B_{\frac{\mu_1 s_i z_i^{\alpha}}{\Omega_i \mu_2 + \mu_1 s_i z_i^{\alpha}}}(\mu_1, \mu_2) . \quad (8)$$

The incomplete Beta function from (6) can be represented by [19; Eq. 8.391]:

$$B_x(p, q) = \int_0^x t^{p-1}(1-t)^{q-1} dt = \frac{x^p}{p} {}_2F_1(p, 1-q; p+1; x) =$$

$$= \frac{x^p}{p} {}_2F_1(a, b; c; z) = \frac{x^p}{p} \sum_{j=0}^{\infty} \frac{a_j b_j}{c_j} \frac{z^j}{j!} , \quad (9)$$

with ${}_2F_1$ beeing the hyper geometric function of the second order.

After a few substitutions, the CDF can be written in the form:

$$F_{z_i}(z_i) = \frac{\Gamma(\mu_1 + \mu_2)}{\mu_1 \Gamma(\mu_1)\Gamma(\mu_2)} \sum_{j=0}^{\infty} \frac{(\mu_1)_j (1-\mu_2)_j}{j!(\mu_1 + 1)_j} \left(\frac{\mu_1 s_i z_i^{\alpha}}{\Omega_i \mu_2 + \mu_1 s_i z_i^{\alpha}}\right)^{j + \mu_1} \quad (10)$$

SC receiver choses the strongest signal from $L$ received signals and processes it (Figure 1). So, the output SIR $z$ is the maximum SIR of all the received SIRs:

$$z = \max(z_1, z_2, ..., z_L) . \quad (11)$$

The PDF of the SIR $z$ at the SC receiver output is [20]:

$$p_z(z) = L p_{z_i}(z_i) \left(F_{z_i}(z_i)\right)^{L-1} . \quad (12)$$

By replacing (4) and (10) into (12), the PDF of the output SIR $z$ becomes:

$$p_z(z) = \frac{L\alpha\mu_2^{\mu_2}}{\mu_1^{L-\mu_1-1}} \cdot \frac{z_i^{\alpha\mu_1 - 1} \Omega_i^{\mu_2} s_i^{\mu_1}}{\left(\Omega_i \mu_2 + \mu_1 s_i z_i^{\alpha}\right)^{\mu_1 + \mu_2}} \left(\frac{\Gamma(\mu_1 + \mu_2)}{\Gamma(\mu_2)\Gamma(\mu_1)}\right)^L \times$$

$$\times \left(\sum_{j=0}^{+\infty} \frac{(\mu_1)_j (1-\mu_2)_j}{(\mu_1 + 1)_j \, j!} \left(\frac{\mu_1 s_i z_i^{\alpha}}{\Omega_i \mu_2 + \mu_1 s_i z_i^{\alpha}}\right)^{j + \mu_1}\right)^{L-1} . \quad (13)$$

### B. Moment Generating Function

The MGF is an important statistical function for each distribution. MGF has many advantages, among which is its usefulness in analysis of sums of Random Variables (RVs). Namely, the MGF of RV gives all moments of this RV, which fact gives the name to the moment generating function. Then, if exists, the MGF determines the distribution uniquely. Therefore, if two RVs have the same MGF, they have the same distribution. Thus, if we find the MGF of a RV, its distribution is determined.

The MGF was introduced for easier determination of the system performance of fading channels in the case of complicated PDF.

In reality, the conditional BEP is a nonlinear function of the SNR or SIR. The nonlinearity is a consequence of the modulation/detection scheme. That is why we consider the MGF-based approach to determine ABEP. So, in the theory of probability and statistics, the MGF of a real RV is an alternate feature of its PDF.

The MGF is defined by formula [21; Eq. (6)]:

$$M_z(h)=\overline{e^{zh}}=\int_0^{\infty} e^{-zh}\,p_{z_i}(z)\,dz\,. \qquad (14)$$

By putting (4) into (14), the MGF for our scenario will be:

$$M_z(h)=\frac{L\alpha\mu_2{}^{\mu_2}\Omega_i{}^{\mu_2}}{\mu_1{}^{L-1}\mu_1{}^{\mu_2}s_i{}^{\mu_2}}\cdot\left(\frac{\Gamma(\mu_1+\mu_2)}{\Gamma(\mu_2)\Gamma(\mu_1)}\right)^L\times$$

$$\times\left(\sum_{j=0}^{+\infty}\frac{(\mu_1)_j(1-\mu_2)_j}{(\mu_1+1)_j\,j!}\right)^{L-1}\times$$

$$\times\int_0^{\infty}\frac{z_i{}^{\frac{2^{\frac{\alpha jL-\alpha j+\alpha\mu_1L}{2}}-1}}e^{-hz}}{\left(\left(\sqrt{\frac{\mu_2\Omega_i}{\mu_1s_i}}\right)^2+\left(z_i{}^{\frac{\alpha}{2}}\right)^2\right)^{1-(j-jL-\mu_1L-\mu_2+1)}}dz\,. \qquad (15)$$

By using the shape [19; Eq. 3.389]:

$$\int_0^{\infty}\frac{x^{2v-1}e^{-\mu x}}{\left(u^2+x^2\right)^{1-q}}dx=\frac{u^{2v+2q-2}}{2\sqrt{\pi}\,\Gamma(1-q)}G_{13}^{31}\left(\frac{\mu^2u^2}{4}\middle|\begin{matrix}1-v\\1-q-v,0,\frac{1}{2}\end{matrix}\right), \qquad (16)$$

into (15), where G[·] represents the Meijer's G-function [19; Eq. 9.301], the MGF for output SIR $z$ becomes:

$$M_z(h)=\frac{L\alpha}{2\sqrt{\pi}\mu_1{}^{L-1}}\left(\frac{\Gamma(\mu_1+\mu_2)}{\Gamma(\mu_2)\Gamma(\mu_1)}\right)^L\left(\frac{\mu_2\Omega_i}{\mu_1s_i}\right)^{\frac{\mu_1L(\alpha-2)}{2}}\cdot$$

$$\times\left(\sum_{j=0}^{+\infty}\frac{(\mu_1)_j(1-\mu_2)_j}{(\mu_1+1)_j\,j!}\left(\frac{\mu_2\Omega_i}{\mu_1s_i}\right)^{\frac{j(\alpha-2)}{2}}\right)^{L-1}\times$$

$$\times\frac{1}{\Gamma(jL-j+\mu_1L+\mu_2)}\times$$

$$\times G_{13}^{31}\left(\frac{h^2\mu_2\Omega_i}{4\mu_1s_i}\middle|\begin{matrix}1-\left(\frac{\alpha jL-\alpha j+\alpha\mu_1L}{2}\right)\\\left(\frac{(2-\alpha)(jL-j+\mu_1L)+2\mu_2}{2}\right),0,\frac{1}{2}\end{matrix}\right). \qquad (17)$$

### C. Average Bit Error Probability

The ABEP is among the system performance of the first order. It describes the system's behavior on the best way. For that reason, simply determining ABEP is of prime importance.

We determine here the MGF-based approach to determine the ABEP for two types of modulations on an efficient way, without numerical integrations.

Based on (17), the ABEP for non-coherent BFSK and BDPSK modulations are [22]:

$$P_{be}(\Omega_0)=0.5M_z(0.5)\,,\quad \text{for BFSK,} \qquad (18)$$

$$P_{be}(\Omega_0)=0.5M_z(1)\,,\quad \text{for BDPSK.} \qquad (19)$$

Follows, we illustrate the influence of fading and CCI severity on the ABEP based on numerically obtained results. For this purpose, we use the programs Origin and Mathematica to plot some figures.

### D. ABEP for Binary Frequency Shift Keying Modulation

Firstly, the case of BFSK modulation is observed. The curves for ABEP versus SIR, $w=\Omega/s$, at the output of the multi-branch SC receiver, when BFSK modulation was used, are shown in Figures 2 and 3. The values for one group of parameters are changed, and the values for the other parameters are kept.

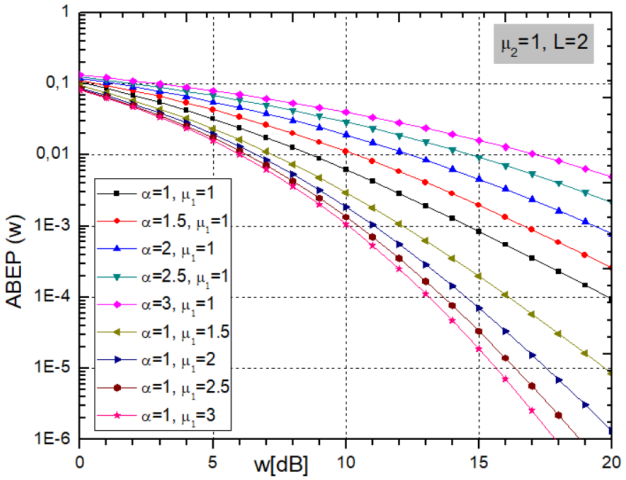


Figure 2. BEP versus SIR for BFSK modulation: parameters α and $\mu_1$ are changing.

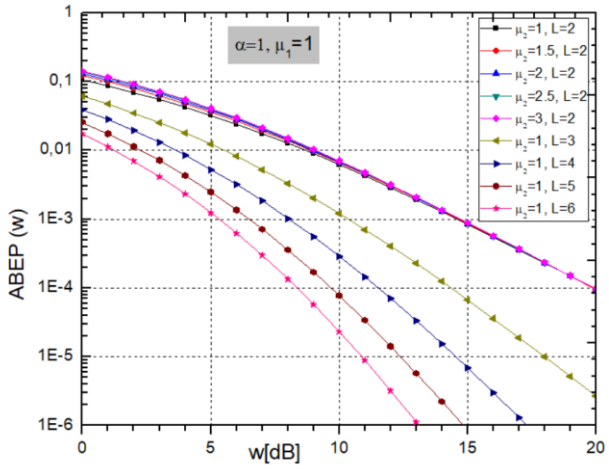


Figure 3. BEP versus SIR for BFSK modulation with variable parameters $\mu_2$ and $L$.

So, in Figure 2, the ABEP is presented for BFSK modulation and dual branch SC receiver ($L$=2), with $\mu_2$=1, while parameters α and $\mu_1$ are changing. One can see from Figure 2 that the ABEP increases with an increasing in parameter α. Then, the system performance becomes worse. When the parameter $\mu_1$ increases, the ABEP decreases and the system has better performance.

In Figure 3, the ABEP is presented versus SIR for BFSK modulation when the parameters $\mu_2$ and $L$ are variable. In this figure, the parameters: α=1, and $\mu_1$=1 have maintained the same values. We can conclude that the increase in the parameter $\mu_2$ has no effect on the ABEP. On the other side, with an increase of the number of branches $L$, the ABEP decreases significantly and the system performance is improved.

### *E. Binary Differential Phase-Shift Keying Modulation*

Now, the case of BDPSK modulation is shown. In Figures 4 and 5, for ABEP for BDPSK modulation is shown versus SIR at the output of SC receiver with $L$ branches. Figure 4 shows graphs for dual branch SC receiver ($L$=2) for $\mu_2$=1, where parameters α and $\mu_1$ took different values. We can remark that the ABEP grows with the increasing of parameter α, spoils the system performance. When the parameter $\mu_1$ increases, the ABEP is decreasing, improving the system performance.

In Figure 5, the ABEP is presented versus SIR for the BDPSK modulation. Here, the values of parameters $\mu_2$ and $L$ are changeable. The parameters that keep their values all the time are: α=1 and $\mu_1$=1. One can see that the increasing of $\mu_2$ is without significant impact on the ABEP. When $L$ (the number of branches) is increasing, the ABEP decreases significantly, and the system performance are improved, which is in accordance with the theory.

When we compare the last two pairs of graphs, we can conclude that the system has smaller ABEP and better performance when BDPSK modulation is used.

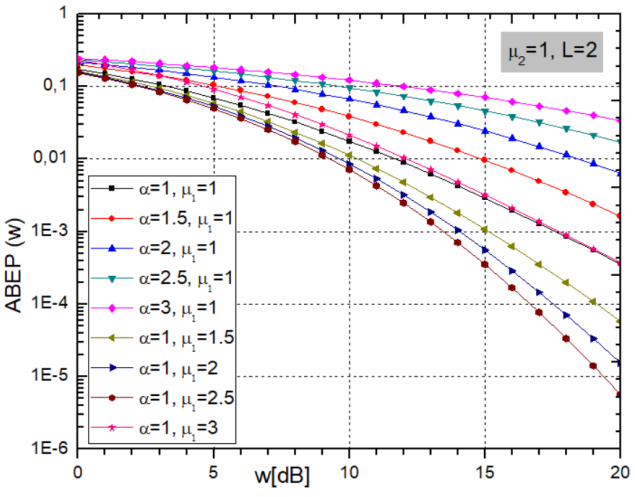


Figure 4. ABEP versus SIR for BDPSK modulation when parameters α and $\mu_1$ are changing.

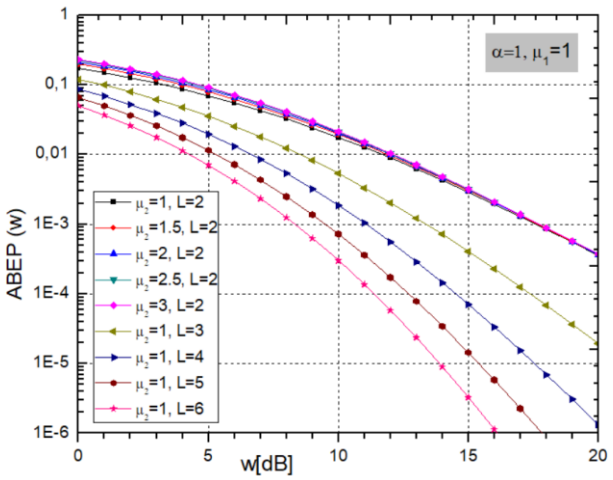


Figure 5. ABEP versus SIR for BDPSK modulation and variable parameters $\mu_2$ and $L$.

## III. SECOND ORDER SYSTEM PERFORMANCE

The LCR is very important the second order performance measure of wireless communication system. It presents the number of crossing the specified level in positive or negative direction. The LCR is being calculated as average value of the first derivative of random process (RP). The AFD is also second order performance measure and is defined as average time that signal envelope is below that specified threshold level. It can be evaluated as the ratio of the Pout and the LCR.

### *A. Level Crossing Rate*

Let now calculate the first derivative of $z_i$, which we need to calculate the LCR:

$$\dot{z}_i = \frac{1}{y_i}\dot{x}_i - \frac{x_i}{y_i^2}\dot{y}_i \,. \tag{20}$$

The derivative of the α-μ RP is a Gaussian RP, and a linear combination of Gaussian processes is also a Gaussian RP. Then, the conditional Gaussian distributed $\dot{z}_i$, with zero mean, has the variance:

$$\sigma_{\dot{z}_i}^2 = \frac{1}{y_i^2}\sigma_{\dot{x}_i}^2 + \frac{x_i^2}{y_i^4}\sigma_{\dot{y}_i}^2 \quad . \tag{21}$$

The variances relating to the signal and interference are [17]:

$$\sigma_{\dot{x}_i}^2 = \left(\frac{2\pi f_m}{\alpha}\right)^2 \frac{\Omega_i x_i^{2-\alpha}}{\mu_1}, \sigma_{\dot{y}_i}^2 = \left(\frac{2\pi f_m}{\alpha}\right)^2 \frac{s_i y_i^{2-\alpha}}{\mu_2} \tag{22}$$

where $f_m$ denotes the Doppler frequency. Unlike [17], we will show here the LCR in the case of different μ values for the signal and CCI: $\mu_1$ for the signal, and $\mu_2$ for the CCI.

After replacing expressions from (22) into (21), the variance $\dot{z}_i$ becomes:

$$\sigma_{\dot{z}_i}^2 = \frac{1}{z_i^{\alpha-2} y_i^{\alpha}} \left(\frac{2\pi f_m}{\alpha}\right)^2 \left(\frac{\Omega_i}{\mu_1} + z_i^{\alpha} \frac{s_i}{\mu_2}\right) \quad (23)$$

The conditional probability density functions (CPDF) of $\dot{z}_i$ and $z_i$ are [18]:

$$p_{\dot{z}_i}\left(\dot{z}_i \middle| z_i y\right) = \frac{1}{\sqrt{2\pi}\sigma_{\dot{z}_i}} e^{-\frac{\dot{z}_i^2}{2\sigma_{\dot{z}_i}^2}},$$

$$p_{z_i}\left(z_i \middle| y_i\right) = \left|\frac{dx_i}{dz_i}\right| p_{x_i}\left(z_i y_i\right) = y_i p_{x_i}\left(z_i y_i\right) \quad (24)$$

The conditional joint probability density function (CJPDF) of $z_i$, $\dot{z}_i$ and $y_i$ is [18]:

$$p_{\dot{z}_i z_i y_i}\left(\dot{z}_i z_i y_i\right) = p_{\dot{z}_i}\left(\dot{z}_i \middle| z_i y_i\right) p_{z_i}\left(z_i \middle| y_i\right) p_{y_i}\left(y_i\right) =$$

$$= p_{\dot{z}_i}\left(\dot{z}_i \middle| z_i y_i\right) p_{y_i}\left(y_i\right) y_i p_{x_i}\left(z_i y_i\right) \quad (25)$$

The joint PDF of $z_i$ and $\dot{z}_i$ becomes finally [18]:

$$p_{\dot{z}_i z_i}\left(\dot{z}_i z_i\right) = \int_0^{\infty} p_{\dot{z}_i z_i y_i}\left(\dot{z}_i z_i y_i\right) dy_i \,. \quad (26)$$

The LCR of the SIR at the output of multi-branch SC receiver is actually the mean value of the first derivative of the SIR at the receiver output. So, it is necessary to average the first derivative by an integration [20]:

$$N_{z_i}\left(z_i\right) = \int_0^{\infty} \dot{z}_i p_{\dot{z}_i z_i}\left(\dot{z}_i z_i\right) d\dot{z}_i \quad (27)$$

Substituting the corresponding expressions in (27), we get:

$$N_{z_i}\left(z_i\right) = \int_0^{\infty} dy_i p_{y_i}\left(y_i\right) y_i p_{x_i}\left(z_i y_i\right) \int_0^{\infty} d\dot{z}_i \dot{z}_i \frac{1}{\sqrt{2\pi}\sigma_{\dot{z}_i}} e^{-\frac{\dot{z}_i^2}{2\sigma_{\dot{z}_i}^2}} =$$

$$= \frac{\sqrt{2\pi} f_m z_i^{\frac{2\alpha\mu_1-\alpha}{2}} \left(\mu_2\Omega_i\right)^{\mu_2-\frac{1}{2}} \left(\mu_1 s_i\right)^{\mu_1-\frac{1}{2}} \Gamma\left(\mu_1+\mu_2-1/2\right)}{\left(\mu_2\Omega_i + \mu_1 s_i z_i^{\alpha}\right)^{\mu_1+\mu_2-1} \Gamma\left(\mu_1\right)\Gamma\left(\mu_2\right)} \,. \quad (28)$$

The LCR of the SIR at the output of the multi-branch SC receiver is defined as [23; Eq. (8)]:

$$N_z\left(z\right) = L\left(F_{z_i}\left(z_i\right)\right)^{L-1} N_{z_i}\left(z_i\right) \quad (29)$$

By using equations (10) and (28) in (29), for $i$=1, 2, ..., $L$, LCR of SIR $z$ at the SC receiver output becomes:

$$N_z\left(z\right) = L \frac{\sqrt{2\pi} f_m z_i^{\frac{2\alpha\mu_1-\alpha}{2}} \left(\mu_2\Omega_i\right)^{\mu_2-\frac{1}{2}} \left(\mu_1 s_i\right)^{\mu_1-\frac{1}{2}} \Gamma\left(\mu_1+\mu_2-1/2\right)}{\left(\mu_2\Omega_i + \mu_1 s_i z_i^{\alpha}\right)^{\mu_1+\mu_2-1} \Gamma\left(\mu_1\right)\Gamma\left(\mu_2\right)} \cdot$$

$$\cdot \left(\frac{\Gamma\left(\mu_1+\mu_2\right)}{\mu_1\Gamma\left(\mu_2\right)\Gamma\left(\mu_1\right)} \sum_{j=0}^{+\infty} \frac{\left(\mu_1\right)_j}{j!} \frac{\left(1-\mu_2\right)_j}{\left(\mu_1+1\right)_j} \left(\frac{\mu_1 s_i z_i^{\alpha}}{\Omega_i\mu_2 + \mu_1 s_i z_i^{\alpha}}\right)^{j+\mu_1}\right)^{L-1} \quad (30)$$

To explore the influence of fading and CCI severity on the concerned LCR, numerically obtained results in (30) are drawn in a few graphs. Figures 6 and 7 show normalized LCR depending on receiver output SIR $z$.

From Figure 6 is visible that when the parameter α increases, the curves of LRC narrow and the maximum of LCR curves increase.

Also, it is notable that LCR decreases for bigger values of parameter α. Further, an increasing of the parameter $\mu_1$ for $z$<0 leads to decreasing of LCR what provides better performance for wireless system. For $z$>0, the parameter $\mu_1$ slightly affects the LCR value.

The next figure, Figure 7 shows that at positive values of $z$ [dB], the LCR increases as the number of branches $L$ at the receiver input increases, and decreases for negative values of $z$, when the system has better performance.

When the parameter $\mu_2$ increases for positive values of $z$, the LCR decreases and the system is improved. The influence of the parameter $\mu_2$ is negligible for negative values of $z$.

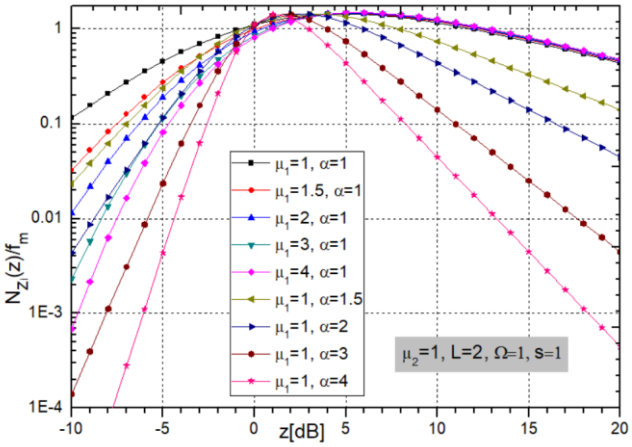


Figure 6. Normalized LCR versus SIR for variable parameters $\mu_1$ and α.

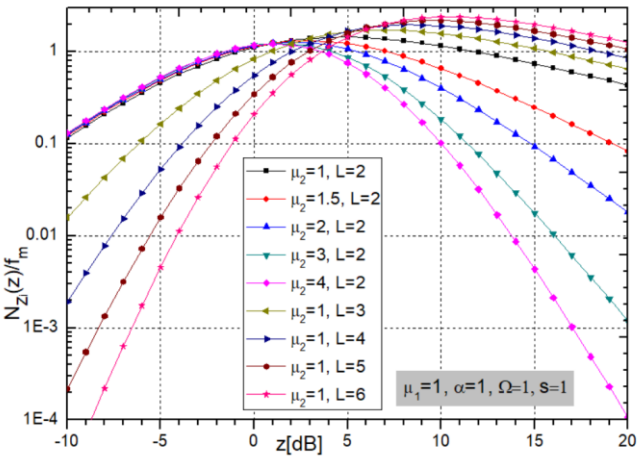


Figure 7. Normalized LCR of defined SC receiver versus SIR for variable parameter $\mu_2$ and number of brunches $L$.

### B. *Average Fade Duration*

For a fading signal, the AFD is defined as the average time over which the signal envelope, or SIR, remains below a certain level. As mentioned above, AFD is equal to the ratio of the Pout and the LCR [24; Eq. 2.106]:

$$AFD = \frac{F_z(z)}{N_z(z)}. \tag{31}$$

Mathematically, Pout is equal to the CDF of SIR $z$ at the output of SC receiver [25]:

$$P_{out} = F_z(z) = \left(F_{z_i}(z_i)\right)^L \tag{32}$$

Since the CDF of $z_i$, $i$=1,2, …, $L$, is given by (10), Pout becomes after replacing:

$$P_{out} = \left( \frac{\Gamma(\mu_1+\mu_2)}{\mu_1\Gamma(\mu_1)\Gamma(\mu_2)} \sum_{j=0}^{\infty} \frac{(\mu_1)_j (1-\mu_2)_j}{j!(\mu_1+1)_j} \left( \frac{\mu_1 s_i z_i^{\alpha}}{\Omega_i \mu_2 + \mu_1 s_i z_i^{\alpha}} \right)^{j+\mu_1} \right)^L \tag{33}$$

The graphics for Pout for the system model described here are presented in [15; Fig. 3] for $\mu_1=\mu_2=\mu$.

Now, by replacing the corresponding expressions for $F_z(z)$ from (32) and $N_z(z)$ from (29), we get AFD:

$$AFD = \frac{\left(F_{z_i}(z_i)\right)^L}{LN_{z_i}(z_i)\left(F_{z_i}(z_i)\right)^{L-1}} =$$

$$= \frac{\Gamma(\mu_1+\mu_2)\left(\mu_2\Omega_i + \mu_1 s_i z_i^{\alpha}\right)^{\mu_1+\mu_2-1} \sum_{j=0}^{\infty} \frac{(\mu_1)_j (1-\mu_2)_j}{j!(\mu_1+1)_j} \left( \frac{\mu_1 s_i z_i^{\alpha}}{\Omega_i \mu_2 + \mu_1 s_i z_i^{\alpha}} \right)^{j+\mu_1}}{L\mu_1\sqrt{2\pi} f_m z_i^{\frac{2\alpha\mu_1-\alpha}{2}} (\mu_2\Omega_i)^{\mu_2-\frac{1}{2}} (\mu_1 s_i)^{\mu_1-\frac{1}{2}} \Gamma(\mu_1+\mu_2-1/2)} \tag{34}$$

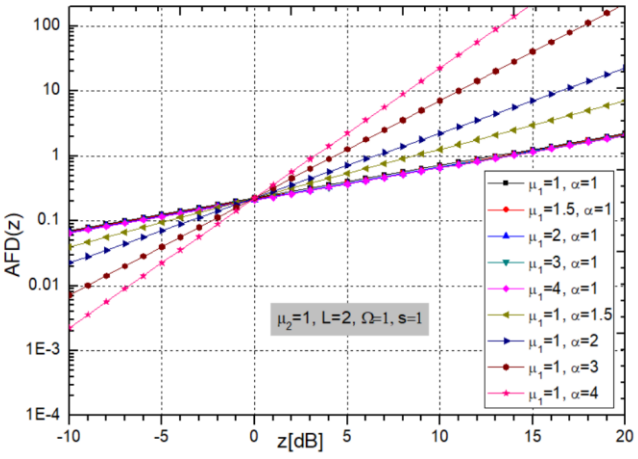


Figure 8. Normalized *AFD* of *L*-branch SC receiver depending on SIR considering different values of fading parameters $\mu_1$ and α.

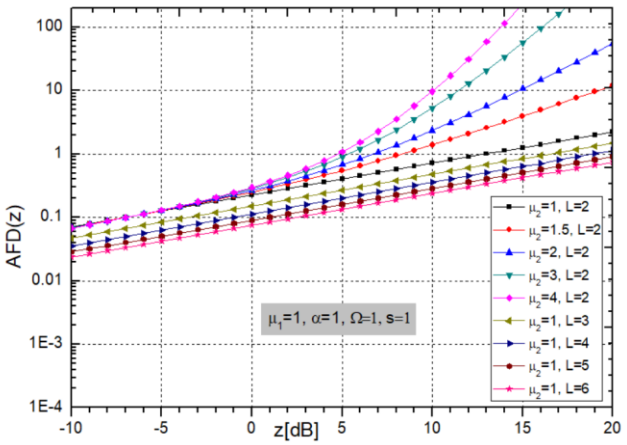


Figure 9. Normalized AFD depending on SIR for variable parameters $\mu_2$ and $L$.

Because of fluctuation of wireless channel, signal amplitude, or SIR, also fluctuates, and the receiver will experience periods during which the signal cannot be reliably detected. The normalized AFDs are presented for various system parameters in Figures 8 and 9.

When the crossing threshold z is below the average signal level, the AFD is low, and this is generally the regime in which the system operates normally. It is obvious from Figure 8 that the AFD gets smaller for bigger α when $z$<0. The AFD increases with increasing the parameter α for $z$>0, and the performance is worse. This figure shows that the size of the parameter $\mu_1$ slightly changes AFD.

From Figure 9 one can conclude that with the growth of $L$ the AFD decreases and system performance is improved. The performance improvement in less severe environments is expected as the number of branches $L$ increases and consequently AFD decreases. On the other side, when the parameter $\mu_2$ increases, in the case of the CCI, the AFD also increases slightly, which is bad for system performance.

## IV. CHANNEL CAPACITY

Channel capacity is of great importance between performance metrics of wireless system. CC is defined as [26]:

$$\frac{CC}{B} = \frac{1}{\ln(2)} \int_0^{\infty} \ln(1+z) p_z(z)\, dz, \tag{35}$$

where $CC$ is Shannon capacity (in bits/s), and $B$ is transmission bandwidth (in Hz).

Deriving an expression for CC is shown in [16]. Unlike the paper [16], here we have introduced different values of parameters $\mu_1$ and $\mu_2$. We give new expression obtained by the procedure in [16].

Final form of CC is:

$$CC = \frac{L}{\ln(2)\mu_1^{L-1}}\left(\frac{\Gamma(\mu_1+\mu_2)}{\Gamma(\mu_2)\Gamma(\mu_1)}\right)^L \sum_{j_1=0}^{+\infty}\frac{(-1)^{j_1}}{(j_1+1)!}\left(\frac{\mu_2}{\mu_1}\left(\frac{\Omega_i}{s_i}\right)\right)^{\frac{j_1+1}{\alpha}} \times$$

$$\times\left(\left(\sum_{j_2=0}^{+\infty}\frac{(\mu_1)_{j_2}(1-\mu_2)_{j_2}}{(\mu_1+1)_{j_2}\,j_2!}\right)^{L-1} B\left(\frac{j_1+\alpha j_2(L-1)+\alpha L\mu_1+1}{\alpha},\frac{\alpha\mu_2-j_1-1}{\alpha}\right)\right) \quad (36)$$

Then, in Figures 10 and 11, we show new graphics for the case of changing these different parameters $\mu_1$ and $\mu_2$, as well as parameter α and number of branches at the receiver input, *L*.

Figure 10 shows the normalized channel capacity for different values of fading parameters $\mu_1$ and α. From this figure, it can be seen that the change of the parameter $\mu_1$ has an insignificant effect on the CC, while when the parameter α increases, the CC decreases and the system has worse performance.

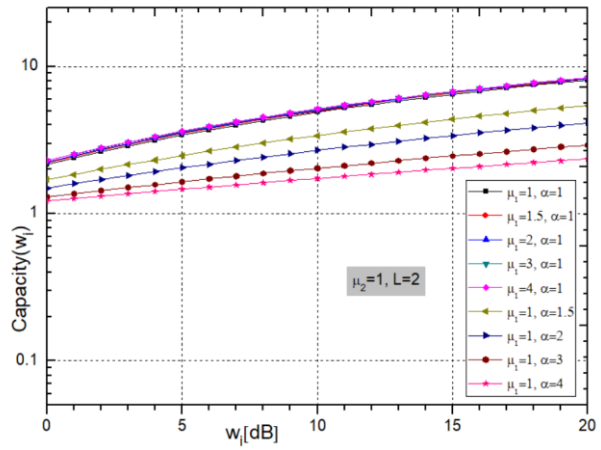


Figure 10. The normalized capacity for the use of SC receiver when the parameters $\mu_1$ and α are changing.

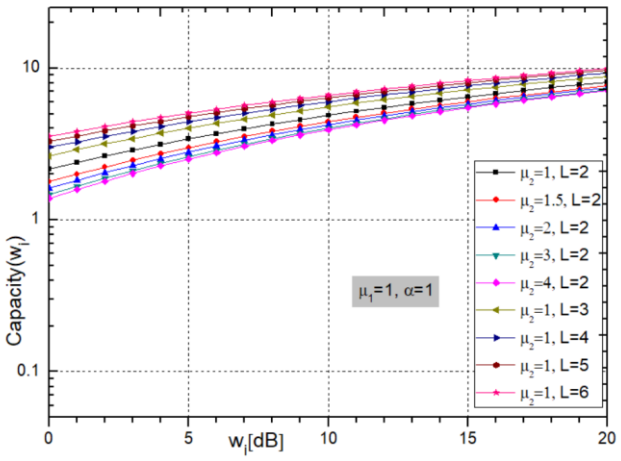


Figure 11. Normalized channel capacity for different values of CCI parameter $\mu_2$ and number of branches *L*.

Figure 11 shows the normalized CC for some values of the CCI parameter $\mu_2$ and variable number of input branches *L*. Other parameters have constant values $\mu_1 = \alpha = 1$. From this figure it can be seen that when $\mu_2$ increases, the channel capacity decreases and the system performs worse. When the number *L* increases, then the channel capacity increases and the system has better performance, which is realistic to expect for a larger number of input branches of the SC receiver.

## V. LLM-ENABLED WIRELESS NETWORK PLANNING WORKFLOW

Since the rise of ChatGPT [27] in late 2022, LLMs have drawn large attention, resulting in various innovative usage scenarios beside human-alike question answering – from poetry writing to playing board games. Based on experiments of many enthusiasts and researchers, it was concluded that LLMs show high potential for many use cases in area of software and computer applications [28]. One of them refers to synergy with model-driven engineering, which comes from the summarization power of LLMs [29]. This way, many novel use cases can be achieved [28]-[30]: 1) metamodel creation - domain conceptualization based on free-form text as input, resulting with metamodel as output; 2) model instance creation - using metamodel and text as input, resulting with model instance as outcome; 3) constraint rule extraction – identifying formal logic rules that should hold within the model instances, based on text and metamodel as inputs as well 4) code generation – parametrized model instances and code templates as input are leveraged to generate the target platform executable code.

Taking into account the previously mentioned scenarios, our aim in this paper is to make use of LLM and MDE synergy in order to reduce the cognitive load when it comes to experimentation in area of mobile and wireless networks. Considering the increasing infrastructure complexity, together with large number of devices involved and their heterogeneity, experimentation aiming prototyping and development of next-generation wireless and mobile networks becomes quite challenging [28], [31]. Therefore, we propose an approach based on MDE technologies for domain concept representation (Eclipse Modeling Framework's Ecore [32]) and ChatGPT, - LLM-based service that enables automated creation of model instances and code generation.

The proposed workflow is illustrated in Figure 12. In the first step, user provides free-form text describing the experiment configuration, together with experiment constraints – both related to network design and performance aspects.

After that, considering user input and meta-model on the other side, the prompt for LLM is constructed in the following form:

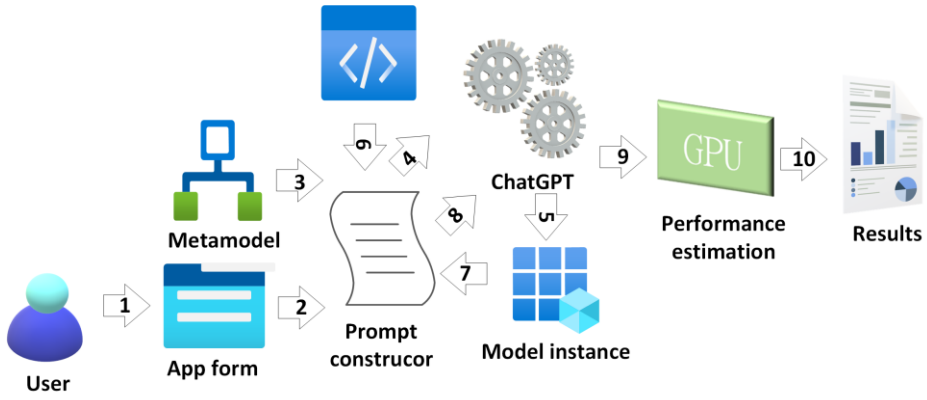


Figure 12. LLM-enabled experimental workflow for next-generation network planning: 1-Experiment definition in free-form text 2-Forwarding user-defined experiment to Prompt constructor 3-Ecore representation of metamodel 4-Prompt1 5-Generated XMI model instance 6-Experiment script Docker template 7-Taking model instance as input for code generation 8-Prompt2 9-Parametrized experiment 11-Performance estimations, such as ABEP.

*Prompt1: Based on description {Experiment text} generate Ecore model instance with respect to metamodel {Ecore metamodel}*

Prompting engine is written in Python programming language, making use of OpenAI Application Programming Interface (API) for ChatGPT. The outcome of this prompt is model instance representing experiment configuration with respect to the given metamodel.

Moreover, based on the provided model parameters, performance estimation is done with respect to performance calculation formulas taking into account the specified fading environment, such as the ABEP expression derived in this paper. For purpose of calculation acceleration, we make use of GPU-enabled approach which introduces high degree of loop-based calculation parallelization, built upon our works from [33]. In order to achieve this, we construct the prompt whose goal is to parametrize experiment script run inside Docker container (by assigning values to environment variables), taking into account the model instance parameters:

*Prompt2: Parametrize template {experiment template} based on model instance {model instance}*

Based on performance estimation results, model instance is augmented with performance-related aspects, so it can be checked from perspective of the desired goals as well. The underlying metamodel used for experiments is depicted in Figure 13.

The highest-level concept is network deployment. It consists of service provider infrastructure elements, such as base stations and service consumers, on the other side, leveraging different receiver types.

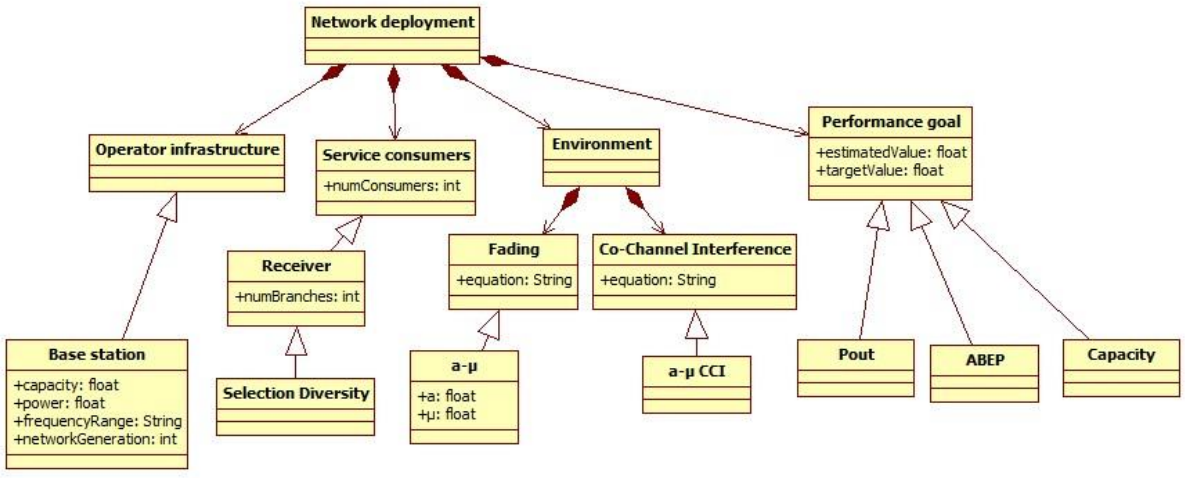


Figure 13. Network experimentation metamodel.

TABLE I. LLM-ENBLED WORKFLOW EVALUATIONAPPROACH EVALUATION

| Aspect | Manual efforts | Execution time [s] | Experiment description |
|---|---|---|---|
| Text to model instance | 50s – Typing the sentence | 7.5 | α-μ fading, α-μ CCI, ABEP 1 receiver/ 2 receivers |
| | | 12.1 | |
| Model instance to experiment | Entirely automatic | 3.3 | |
| | | 8.2 | |
| Performance estimation | Entirely automatic | 1.5 | |
| | | 2.4 | |

For telco infrastructure, we take into account their power consumption, frequency range, capacity in terms of user number and targeted network generation (2G-5G). Additionally, environmental aspects are taken into account as well in form of fading and co-channel interference type, where each specific type has distinct parameters. Finally, the model takes also into account performance-related goals which are taken into account, such as boundary values for ABEP, channel capacity or outage probability. The estimated performance value is compared to these goals in the end, so user will be notified whether the proposed deployment satisfies the requirements.

Table I gives summary of the achieved results for different experiment configurations. Execution time required for various relevant steps is given.

Taking into account that in our previous works knowledge of domain modeling tools was required, the experimental workflow required much more effort and time, up to 10 minutes for a single experiment, speed up is significant.

On the other side, LLM-aided approach significantly reduces the time required for creation of a single experiment and overall cognitive overload, as only freeform text has to be provided by end.

## VI. CONCLUSION

In our work, a wireless system in fading and CCI environment was observed. The both disturbances are described by α-μ distribution. SC diversity technique was used to mitigate the effects of fading and CCI and improve the system performance. To highlight the influence of fading and CCI parameters, all derived analytical results are plotted on some figures. The MGF-based ABEP is obtained for BFSK and BDPSK modulation types. We concluded from presented graphs that, in α-μ environments, more advantageous is using of BDPSK than BFSK modulation. Then, we derived and presented LCR, AFD and CC for defined system model.

The performance derived in this paper can be used for the systems in the presence of known fading and CCI with Rayleigh, Nakagami-*m*, Weibull, and One-sided Gaussian distributions, by setting special values of parameters α and μ in α-μ general distribution.

The proposed approach leveraging LLMs and MDE significantly reduces time and effort needed for wireless network experimentation, requiring only free-from natural language text as input from the end user.

In the future we will consider correlated α-μ channels, as well as other types of fading environments. The correlation between the faded channels affects badly on the PDF of SIR at the output of the receiver. Finally, we would also take into account the adoption of LLMs for purpose of automated model constraint extraction in form of Object Constraint Rules (OCL), so automated model instance consistency checking can be performed in order to verify if it complies to some reference requirements.

## ACKNOWLEDGMENT

This work is done in the frame of the bilateral project "Development of Secure and Spectral Efficient Simultaneous Wireless Information and Power Transfer Systems for Large-Scale Wireless Networks" under Science and Technological Cooperation Projects (2022-2024) between the Republic of Serbia and the Republic of India.

## REFERENCES

[1] D. Krstic, S. Suljovic, D. S. Gurjar, and S. Yadav, "Moment generating function based calculation of average bit error probability in an α-μ fading environment with selection diversity receiver", IARIA Congress 2023, The 2023 IARIA Annual Congress on Frontiers in Science, Technology, Services, and Applications, , Valencia, Spain, November 13, 2023 to November 17, 2023, pp. 203 – 207.

[2] M. D. Yacoub, "The α-μ distribution: a general fading distribution", The 13th IEEE International Symposium on Personal, Indoor and Mobile Radio Communications PIMRC. 2002. Lisboa, Portugal, September 15-18, 2002. doi:10.1109/pimrc.2002.1047298

[3] M. D. Yacoub, "The *α*-μ distribution: a physical fading model for the Stacy distribution", IEEE Transactions on Vehicular Technology, vol. 56, no. 1, pp. 27-34, Jan. 2007. DOI: 10.1109/TVT.2006.883753

[4] M. D. Yacoub, "The κ-μ distribution: a general fading distribution", IEEE 54th Vehicular Technology Conference. VTC Fall 2001. doi:10.1109/vtc.2001.956432

[5] M. D. Yacoub, "The κ-μ distribution and the η-μ distribution," IEEE Antennas and Propagation Magazine, vol. 49, no. 1, pp. 68-81, Feb. 2007, doi: 10.1109/MAP.2007.370983.

[6] G. Fraidenraich and M. D. Yacoub, "The α-η-μ and α-κ-μ Fading Distributions", 2006 IEEE Ninth International Symposium on Spread Spectrum Techniques and Applications, October 2006, DOI: 10.1109/ISSSTA.2006.311725

[7] G. Fraidenraich and M. D. Yacoub, "The λ - μ general fading distribution", The 2003 SBMO/IEEE MTT-S International Microwave and Optoelectronics Conference - IMOC 2003, Foz do Iguacu, Brazil, 20-23 September, 2003, pp. 49-54. doi:10.1109/imoc.2003.1244830

[8] A. Magableh and M. Matalgah,"Moment generating function of the generalized α-μ distribution with applications", IEEE Communications Letters, vol. 13, issue 6, pp. 411–413, June 2009. DOI:10.1109/lcomm.2009.090339

[9] A. M. Magableh and M. M. Matalgah, "Channel characteristics of the generalized alpha-mu multipath fading model", The 7th International Wireless Communications and Mobile Computing Conference, IWCMC 2011, Istanbul, Turkey, 4-8 July, 2011, pp. 1535-1538. DOI: 10.1109/IWCMC.2011.5982766

[10] S. P. Singh, M. Jadon, R. Kumar, and S. Kumar "BER analysis over alpha-mu fading channel using proposed novel MGF", International Journal of Wireless and Mobile Computing, vol. 10, no. 2, pp. 174 – 182, 2016. DOI: 10.1504/IJWMC.2016.076162

[11] W. H. M. Freitas, R. C. D. V. Bomfin, R. A. A. de Souza, and M. D. Yacoub, "The complex α-μ fading channel with OFDM application",

International Journal of Antennas and Propagation, vol. 2017, 2017. https://doi.org/10.1155/2017/2143541

[12] J. T. Ferreira, A. Bekker, F. Marques, and M. Laidlaw, "An enriched α − μ model as fading candidate", Mathematical Problems in Engineering, vol. 2020, 2020. https://doi.org/10.1155/2020/5879413

[13] G. Milovanović, M. Stefanović, S. Panić, J. Anastasov, and D. Krstić, „Statistical analysis of the square ratio of two multivariate exponentially correlated α-μ distributions and its application in telecommunications", Mathematical and Computer Modelling, vol. 54, no. 1-2, pp. 152–159, July 2011. DOI:10.1016/j.mcm.2011.01.046

[14] M. K. Simon and M. S. Alouini, Digital Communication over Fading Channels, 2nd ed. Hoboken, NJ, USA: Wiley-IEEE, 2004.

[15] D. Krstic, S. Suljovic, N. Petrovic, Z. Popovic, and S. Minic, "Derivation, analysis and simulation of outage performance of MIMO multi-branch SC diversity system in α−μ fading and co-channel interference environment", 11th International Conference of Applied Internet and Information Technologies, AIIT 2021, Zrenjanin, Serbia, 15 October, 2021.

[16] D. Krstic, S. Suljovic, N. Petrovic, D. S. Gurjar, S.Yadav, and A. Rastogi, "Quantum machine learning-assisted channel capacity analysis of L−branch SC diversity receiver in α − μ fading and CCI environment", 2022 IEEE Silchar Subsection Conference, (SILCON), Silchar, India, 4-6 November 2022. DOI: 10.1109/SILCON55242.2022.10028953

[17] D. Milić, S. Suljović, D. Rančić, N. Petrović, and N. Milošević, "Performance simulation for LCR of MIMO Multi-branch SC Diversity System in α-μ fading and α-μ interference channel", IX International Conference IcETRAN, Novi Pazar, Serbia, 6 - 9. June 2022, pp. 706-710.

[18] S. Suljović, D. Krstić, D. Bandjur, S. Veljković, and M. Stefanović, "Level crossing rate of macro-diversity system in the presence of fading and co-channel interference", Revue Roumaine des Sciences Techniques, Publisher: Romanian Academy, vol. 64, pp. 63–68, 2019.

[19] I. S. Gradshteyn and I. M. Ryzhik, Tables of Integrals, Series and Products Academic. New York: 1980.

[20] S. Suljović, D. Milić, S. Panić, Č. Stefanović, and M. Stefanović, "Level crossing rate of macro diversity reception in composite Nakagami-*m* and Gamma fading environment with interference", Digital Signal Processing, Vol. 102, July 2020, 102758.

[21] N. C. Sagias and G. K. Karagiannidis, "Gaussian class multivariate Weibull distributions: Theory and applications in fading channels", IEEE Transactions on Information Theory, vol. 51, issue 10, pp. 3608–3619, 2005. DOI: 10.1109/TIT.2005.855598

[22] M. Č. Stefanović, D. M. Milović, A. M. Mitić, and M. M. Jakovljević, "Performance analysis of system with selection combining over correlated Weibull fading channels in the presence of cochannel interference", AEU - International Journal of Electronics and Communications, 62(9), pp. 695–700, 2008. 21

[23] C. Stefanovic, S. Veljković, M. Stefanović, S. Panić, and S. Jovković, "Second order statistics of SIR based macro diversity system for V2I communications over composite fading channels", First International Conference on Secure Cyber Computer and Communication (ICSCCC), Jalandhar, Punjab, India, 15-17 December, 2018, pp. 569-574.

[24] G. L. Stuber, Principles of Mobile Communication, 2nd ed., Kluwer Academic Publisher, 2000.

[25] D. Ben Cheikh Battikh, "Outage probability formulas for cellular networks: contributions for MIMO, CoMP and time reversal features", PhD Thesis, 2012, Telecom ParisTech.

[26] M. S. Alouini and A. J. Goldsmith, "Capacity of Rayleigh fading channels under different adaptive transmission and diversity-combining techniques," IEEE Transactions on Vehicular Technology, vol. 48, no. 4, pp. 1165–1181, 1999.

[27] https://chat.openai.com/, accessed on 22 March 2024.

[28] D. Krstic, N. Petrovic, S. Suljovic, and I. Al-Azzoni, "AI-enabled framework for mobile network experimentation leveraging ChatGPT: case study of channel capacity calculation for η-μ fading and co-channel interference", Electronics 2023, 12, 4088, pp. 1-19, 2023. https://doi.org/10.3390/electronics12194088

[29] N. Petrović and I. Al-Azzoni, "Model-driven smart contract generation leveraging ChatGPT", The 30th International Conference on Systems Engineering, ICSEng 2023, Las Vegas, Nevada, USA August 22-24, 2023. https://doi.org/10.1007/978-3-031-40579-2_37

[30] N. Petrović and I. Al-Azzoni, "Autoamated approach to model-driven engineering leveraging ChatGPT and Ecore", 16th International Conference on Applied Electromagnetics – IIEC 2023, Niš, Serbia, August 28 – 30, 2023, pp. 166-168.

[31] D. Krstić, N. Petrović, and I. Al-Azzoni, "Model-driven approach to fading-aware wireless network planning leveraging multiobjective optimization and deep learning", Mathematical Problems in Engineering, 4140522, 2022. https://doi.org/10.1155/2022/4140522

[32] https://eclipse.dev/modeling/emf/, accessed on 22 March 2024.

[33] N. Petrović, S. Vasić, D. Milić, S. Suljović, and S. Koničanin, "GPU-supported simulation for ABEP and QoS analysis of a combined macro diversity system in a Gamma-shadowed k-μ fading channel", Facta Universitatis, Series: Electronics and Energetics, vol. 34, no. 1, pp. 89-104, March 2021. https://doi.org/10.2298/FUEE2101089P